Identification of leakage and potential areas for internal erosion combining ERT and IP techniques at the Negratín dam left abutment (Granada, southern Spain)

Martínez-Moreno, Francisco José*[a], Delgado-Ramos, Fernando[b,c], Galindo-Zaldívar, Jesús[d,e], Martín-Rosales, Wenceslao[d], López-Chicano, Manuel[d], González-Castillo, Lourdes[d]

[a] Instituto Dom Luiz, Faculdade de Ciências, Universidade de Lisboa, 1749-016 – Lisboa, Portugal (fjmoreno@fc.ul.pt)

[b] Departamento de Mecánica de Estructuras e Ingeniería Hidráulica Universidad de Granada, 18071-Granada, Spain. (fdelgado@ugr.es)

[c] Instituto Universitario de Investigación del Agua Universidad de Granada, 18071-Granada, Spain.

[d] Departamento de Geodinámica, Universidad de Granada, 18071-Granada, Spain. (jgalindo@ugr.es; wmartin@ugr.es; mlopezc@ugr.es; lgcastillo@ugr.es)

[e] Instituto Andaluz de Ciencias de la Tierra, CSIC-Universidad de Granada, 18071-Granada, Spain.

**Corresponding Author: e-mail: fjmoreno@fc.ul.pt. Phone: 00351 911028624*

ABSTRACT

At the Negratín Dam (southern Spain) two main springs derived from the water reservoir were detected on the west side of the mountain ridge, matching the location of the left abutment of the dam. The seepages appear when the level of the stored water exceeds 622 meters above sea level (m a.s.l.), where some paleochannels are embedded in the silts. The water level was at 631 m a.s.l. on the day of the measurements (13/12/23), close to the historical maximum (633.78 m a.s.l.). Although the water crossing the leaks does not drag particles nowadays, this sector may potentially cause internal erosion or piping phenomena implying a loss of water resources and slope instability problems. The infiltration areas were evaluated by electrical resistivity and induced polarization methods, measured along one profile on the mountain ridge between the water reservoir and the springs. We determine that the infiltrations zones

are characterized by low resistivity and high chargeability distributed in small areas. We demonstrate that these methods are a reliable tool to detect and characterize infiltration zones, and they are the first step to planning mitigation actions to avoid the piping phenomena.

Keywords: internal erosion, embankment dam, paleochannels, seepages, concrete cut-off wall.

Highlights

- Leakages were detected close to the left abutment of Negratín Dam.
- Two main springs appear when the reservoir level exceeds 622 m a.s.l.
- Internal erosion can lead to piping and instability problems in the future.
- ERT and IP methods were applied to detect potential areas of internal erosion.
- Low resistivity and high chargeability zones indicate preferential leakage routes.

1. Introduction

Internal erosion is a major cause of embankment dam failure (Fell *et al.*, 2003; Gutierrez *et al.*, 2015). It occurs when soil particles within an embankment dam or its foundation are dragged downstream by seepage flow, owing to the erosive forces imposed by hydraulic loads that exceed the resistance of the materials. Thus, the erosive power is directly related to reservoir water level. Most internal erosion processes appear on first filling, but they may also occur during operational years after refilling (Turkmen, 2003; Ghobadi *et al.*, 2005; Uromeihy and Barzegari, 2007; Unal *et al.*, 2007).

A number of earth dam failures in the nineteenth and twentieth centuries can be traced to internal erosion, although piping occurs since approximately 1900 BC with the first earth dam constructions (Richards and Reddly, 2007). Historical dam failure has been addressed by a number of piping research studies (Richards and Reddy, 2007; Atallah *et al.*, 2015; Wang *et al.*, 2016).

The process can be summed up as follows (Richards and Reddly, 2007): (i) particles are progressively dislodged from the soil matrix through tractive forces produced by intergranular seeping water; (ii) erosion is due to flow along pre-existing openings such as cracks in cohesive material or voids along underground structures; (iii) rainfall erosion causes ‘tunneling’ or ‘jugging’, common features perceived in dispersive soils, and it occurs within the vadose zone due to chemical dispersion of clay soils from rainwater; (iv) the process defined as ‘suffusion’ consists of the loose framework of granular material with relatively high seepage flows that results in collapses of the soil structure; (v) the term ‘heave’ in piping phenomena means that a semipermeable barrier overlies a permeable zone under relatively high fluid pressures.

64 There are more than 250 historical cases of piping in earth dams (according to Jones
65 and Trudgill, 1981; reviewed by Richard and Reddy, 2007). In most the piping is
66 produced along conduit and other internal structures (~50% of the historical cases),
67 followed by backward erosion (>31%), along foundations or abutments (~15%) and
68 finally by biological activity (<5%). The most famous case of piping phenomena was
69 produced in the Teton Dam (USA) in 1976 while the first filling was under way (Seed
70 and Duncan, 1987; Smalley and Dijkstra, 1991).

71 The first step in mitigating the problem is to detect the infiltrations. Geophysical
72 methods such as electrical resistivity tomography (ERT), induced polarization (IP) and
73 self-potential (SP) can detect areas prone to infiltration, thereby helping prevent or
74 remedy leakage or piping phenomena in earth dams (Panthulu *et al.*, 2001; Marescot *et*
75 *al.*, 2008; Perrone *et al.*, 2014).

76 Electrical resistivity methods measure the resistivity distribution underground, and IP
77 can detect material capable of retaining the electrical current for a short period of time,
78 such as metallic minerals and clays (Daily *et al.*, 2004). ERT has been successfully
79 employed to detect underground water movements (Slater *et al.*, 2002), environmental
80 remediation (LaBrecque *et al.*, 1996), water-table in several geological settings
81 (Martínez-Moreno *et al.*, 2013) and to evaluate seepage flow rates indirectly in
82 combination with temperature. IP can be used to complement the resistivity method
83 detecting clays within an aquifer (Martínez-Moreno *et al.*, 2013) or metallic
84 mineralizations (Martinez-Moreno *et al.*, 2014). Indeed, combining the two methods
85 gives the best-fitted results (Karaoulis *et al.*, 2014), and both has been applied in the
86 study of dam embankments (Akande, 2016; Loperte *et al.*, 2016).

87 If erosion occurs and fine particles are removed, resistivity is affected in two ways:
88 (i) porosity increases, which decreases the resistivity, (ii) the reduction in fine contents

89 increases the resistivity; but the water conductivity must be also taken into account.
90 Once internal erosion begins, the eroded particles are transported and may be deposited
91 or trapped downstream. Therefore, the presence of clay particles in an area where the
92 soils originally do not contain them could be another signal of internal erosion
93 upstream.

94 The Negratín Dam (southern Spain) presents a determined number of leakages
95 throughout the mountain ridge forming the left abutment of the reservoir. These leaks
96 appear when the water level exceeds the 622 m above sea level (a.s.l.) by the presence
97 of paleochannels embedded in the substratum. These infiltrations not drags particles
98 although they can derive in piping and/or internal erosion in the near future.

99 Concerning to the above exposed problems, this study aims to detect preferential
100 leakage routes and the initiation of internal erosion in the Negratín Dam, close to the left
101 abutment, by measuring electrical resistivity and induced polarization along a profile.
102 This case is quite unusual due to where leakages have been detected is not an
103 embankment dam or its foundation, but a natural mountain ridge between two parallel
104 ravines close to the left abutment of the dam. In addition, ERT and IP combined have
105 not been used to detect this kind of infiltrations in such contexts.

106 **2. Geological framework and Negratín Dam setting**

107 *2.1 Geological framework*

108 The Negratín Dam is located on the western edge of the Guadix-Baza intramontane
109 basin, within the central sector of the Betic Cordillera (southern Spain). The area
110 includes Pliocene lacustrine and alluvial sediments, respectively within the central and
111 marginal areas (Alfaro *et al.*, 1997; Soria *et al.*, 1999).

112 The area surrounding the dam (Fig. 1) includes lithologies from the Miocene at the
113 base (bioclastic limestones, marls and sandstones) and sediments from the Pliocene
114 (conglomerates, clays, gravels and sands), while the *Guadix formation* (Viseras, 1991;
115 Vera *et al.*, 1994) above contains conglomerates, clays (lutites) and sands distributed in
116 an irregular alternating sequence. Finally, Quaternary gravels, silts and sands constitute
117 the top. The general bedding of the area dips 10º to the SE.

118 The local geological structure of the dam consists of Triassic substrate (Keuper) with
119 red clays and gypsum, and a Pliocene and Miocene filling of Helvetian sandstones in
120 the center and the right abutment; marls and sandstones belonging to the late Miocene
121 are found in the left abutment. The top of the local sequence contains silts, sands and
122 gravels from the Quaternary (Fig. 1b). This geological asymmetry creates a mixed dam
123 typology: close to the right abutment, there is a gravity dam with spillways and outlets,
124 and near the left one there is asphalt concrete facing the embankment dam.

125 The left abutment of the dam is a low mountain ridge elongated in the same direction
126 as the dam. This crest acts as a natural embankment dam, but its geological structure is
127 very favorable to water leakage. A section (Fig. 1b) shows a sedimentary sequence with
128 the *Guadix Formation* (quite impervious clays and conglomerates) covered by
129 alternating gravel, sands and silts, containing paleochannels.

130 One of the boreholes drilled in this area (Fig. 1c) reveals that the uppermost sediment
131 has layers about 1 m thick of gravels and sands (Pleistocene paleochannels) within the
132 Quaternary sedimentary package (Fig. 2). They are distributed throughout the study area
133 and present different dimensions, from a few meters (Fig. 2a) to decametric sizes (Fig.
134 2b). It is remarkable that within the paleochannels the presence of clay is negligible.

135 *2.2 The Negratín Dam*

136 The Negratín Dam was built across the Guadiana Menor River (Fig. 1a), a tributary
137 of the Guadalquivir River. The reservoir capacity is 567 hm^3 and the average annual
138 run-off is just 292 hm^3, making it a year-to-year reservoir. The first filling started in
139 1985 when the water level was located at 575.5 m a.s.l. In February 1997, the water
140 level exceeded 622 m a.s.l. and several springs appeared in the natural hill located from
141 400 to 900 meters away –SW of the left abutment (Fig. 3)– where some paleochannels
142 are located. In May 1998, the reservoir reached its historical maximum level of 633.78
143 m a.s.l. –only 3.72 meters below the maximum capacity. Leakage increased up to a flow
144 rate of 17.5 l/s, and several landslides occurred downstream of the natural ridge.

145 In order to reduce the risk of landslides and internal erosion, a concrete cut-off wall
146 of 130-meter long, 0.8 m wide and variable profundity (from 5 to 32 m) to penetrate 5
147 m in the impermeable substratum was built between November 1997 and June 1998
148 (Fig. 3b, 900 m away from the dam). This concrete cut-off wall includes rebar. It was
149 accompanied by a grout curtain from the concrete cut-off wall to the dam left abutment,
150 which comprises the total extension of the ERT profile in Fig. 3. However, these
151 constructions were not enough to avoid water leakage through the two main springs
152 located at ~618 m a.s.l. and separated ~100 m (Fig. 3b).

153 From August 2005 to March 2009 (a dry period) the reservoir level was below 622 m
154 a.s.l., and leakages stopped. In 2007 the *Guadalquivir Hydrographic Confederation*
155 (CHG) planned to complete the concrete cut-off wall, connecting the existing one with
156 the dam. The planned wall was to have a length of 856.5 m, a thickness of 0.80 m and a
157 variable depth, from 5 to 35 meters. However, the project was never executed.

158 Then the water level of the Negratín reservoir rose again. In March 2010, February
159 2011, March 2013 and April 2014 the water level exceeded 632 m a.s.l. (Fig. 4) and the
160 leakages flow rate increased quickly. Therefore, the CHG decided to partly drawdown

161 the water level of the reservoir in 2014 updating the project involving the new concrete
162 cut-off wall. There are still doubts about how deep and long the new cut-off wall should
163 be. Geophysical techniques provides highly useful information about the optimal limits
164 for construction of the cut-off wall.

165 On December 23th, 2013, an electrical profile was measured to acquire resistivity and
166 induced polarization data. The repetition of new measurement to evaluate the evolution
167 of the leaks is not possible due to the drawdown of the water level and the drought
168 period (see Fig. 4).

169 **3. Electrical methods**

170 Electrical methods serve to determine the resistivity distribution underground and
171 detect elements with induced polarization properties –mainly clays associated with
172 water flow through leaks. The electrical profile was acquired using a Terrameter SAS
173 4000 (ABEM, Inc.). The mechanism consists of electrical current injection by a pair of
174 steel electrodes to measure the potential difference. After injecting current to measure
175 the resistivity underground, the equipment stops injection and measures the IP, with a
176 transient voltage decay in a number of time intervals. The resolution of the equipment is
177 about ±1 μV.

178 The profile was acquired with a 4-channel multiple gradient electrode array. The
179 gradient protocol uses an '*alfa*' type electrode arrangement where the potential
180 electrodes are between the current ones (Loke, 2016). This array was developed for a
181 multi-channel resistivity meter system (Dahlin and Zhou, 2006).

182 The profile was measured on December 23th, 2013 with 450 m long in a NNW-SSE
183 direction (Fig. 3) and an electrode spacing of 2.5 m. The depth reached was ~40 m,
184 from 640 until 600 m a.s.l., which comprises the infiltration area because the leaks

appear at 622 m a.s.l. The number of data points acquired for the profile was 3550, applying 5 times the roll-a-long technique, with increments of 50 m for each of them.

The inversion data were calculated using RES2DINV software v.3.59 (Geotomo Inc.), by means of a standard least-square inversion method (deGroot-Hedlin and Constable, 1990; Sasaki, 1992; Loke *et al.*, 2003), and model refinement constraint due to the large amount of data. A mesh made-up of model cells was applied, increasing the size at greater depth, with 4-nodes per unit electrode spacing. The inversion was carried out using finite element.

The depth of investigation (DOI) index indicates the profundity to which the inversion results are reliable. In calculating the empirical DOI (Marescot *et al.*, 2003; Oldenburg and Li, 1999) two data inversions are carried out using different resistivity backgrounds (Loke, 2016). The main difficulty for computing the normalized empirical DOI lies in deciding the cut-off value where the results are reliable. Marescot *et al.* (2003) recommend a value of 0.1 or 0.2, so that we chose the more restrictive value of 0.1. This means that the area above the cut-off value would be fully consistent with measured data (Robert *et al.*, 2011; Martínez-Moreno *et al.*, 2015).

The electrical profiles were acquired on December 23th, 2013, with the reservoir level at 631 m a.s.l., almost 3 meters below the maximum historical water level, and 9 meters above the level where the springs are activated. The water temperature was 11.5 ºC and the electrical conductivity at 25º was 1175 µS/cm.

4. Electrical results

The resistivity model highlights three differentiated areas (Fig. 5). The shallow layer –10 meters from the surface up to ~630 m a.s.l.– detects values over 2000 ohm×meter (Ω·m). This high resistivity is disrupted at 190-220 and 260 m length, where low

resistivity values are detected (~5 Ω·m) matching with the location of the ravine. A second layer located between 620-630 m a.s.l. presents intermediate resistivity about 50 Ω·m and contains specific areas with ~10 Ω·m. The deepest part of the ERT profile registers a resistivity of ~100 Ω·m, including a low resistive zone located at 275 m length. The described layers have the same order, thicknesses and values at the highest topographical part of the profile, at a distance of 290-380 length, although the depth varies. At the end of the profile, from 400 to 450 m length, there are lateral changes from high to low resistivity due to the presence of the concrete cut-off wall (see location with respect to the profile in Fig. 3), since it contains iron embedded in the concrete structure.

The model of induced polarization presents three zones with distinctively high chargeability. The first one is located at a distance of 120 length and from 620 to 630 m a.s.l., reaching values around 12 milliseconds (msec). The strongest chargeability is located at 240-260 m length in the deepest part of the profile, with a chargeability higher than 15 msec. Finally, from 380 to 400 m length is registered an area with values of ~12 msec. Further small areas present intermediate chargeability values considered irrelevant for the case of study.

For both models, the line that defines the 0.1 cut-off value of the DOI index is located below and outside the profile, so that the entire pseudosections are relied on for interpretation. The inversion root mean square (RMS) error in the resistivity model is less than 10%, which is acceptable. However, the error of the IP model is 23.3%. Considering the great amount of inverted data (3500 data points), high RMS errors are usually obtained and the models are tolerable.

5. Discussion

5.1 Geological and geophysical interpretation

Integrated interpretation of the data was intended to distinguish seepages along the hill. The aim was to detect preferential infiltration areas and zones with a higher risk of internal erosion and/or piping.

The geological cross section is shown over resistivity and IP models in Figure 6. The water level below which the leakages disappear is marked (~622 m a.s.l.) along with the water level on the day of measurement (~631 m a.s.l.; 13/12/23). The area above the current water level shows very high resistivity belonging to the vadose zone. It also has a very low chargeability due to the absence of clays. To the contrary, the area below the current water level shows lower resistivity values with elliptical shapes (zones 1, 2 and 3). These three zones are located close to the reservoir level where the leakages are reactivated (~622 m a.s.l.). They are placed above the Guadix formation and the layer of gravels at the contact between the Guadix formation and the Quaternary sediments.

Bearing in mind that this area was grouted, the elliptical zones with very low resistivity may correspond to poorly grouted paleochannels where concentrated leakages occur. Yet a single interpretation of the resistivity model does not provide specific information about the areas where the internal erosion processes may take place. There are other zones with similar resistivity values where infiltrations are not taking place. Therefore, to avoid misinterpretations, a joint analysis was needed, including ERT and IP results, because when infiltration happens the water drags clay particles that remain within the leaks ducts. The presence of clays gives rise to high chargeability values in the IP model (Marescot et al., 2008; Leroy and Revil, 2009; Martínez-Moreno *et al.*, 2013). Three zones were identified with these characteristics between 622 and 631 m a.s.l.: at a distance of 90, 125 and 240 in length (marked 1, 2 and 3 in Fig. 6). It must be taken into account that the IP model does not accurately

represent the shape of the detected structures or their precise position (Martínez-Moreno *et al.*, 2014).

The electrical profile marks other geological structures, such as the one located at a distance of 280 length, where there is an area in depth having low resistivity and high chargeability. This vertical structure is associated with the regional fault that crosses the profile (see Fig. 1) and it causes clay accumulation at the fracture surface (Suzuki *et al.*, 2000). However, this structure does not favour the water infiltration observed at the W side of the mountain ridge (Fig. 3), since it acts as an impervious barrier. Moreover, the concrete cut-off wall (Figs. 3 and 6) is highlighted as low resistivity and high chargeability zones –although the chargeability values are displaced to the NNW– due to the iron bars embedded in the concrete.

In order to evaluate internal erosion through leakage and its evolution, it would be appropriate to repeat the geophysical measures at different times. Yet because the reservoir level was dropped below 622 m a.s.l. in 2016 and the leakages disappeared, it was necessary to find an alternative approach, not waiting until another wet period. Thus, all currently available information aided in decision-making. In this kind of studies, it is recommended to perform monitoring of the dam embankments to determine the infiltrations degree, its evolution and piping development. These are potential methods because exists resistivity contrast between dry and infiltrated areas, and the dragged clays are well detected in the IP method. However, they may present limitations since it depends on the level of water reservoir (above the leaks areas) to have the mentioned resistivity contrasts.

For the time being, no turbidity or deposits of eroded particles had been observed in the springs; some areas covered by vegetation may have hidden the potential deposits from internal erosion. Gravels above the contact with the Guadix Formation and the

paleochannels would be the most favorable zones for the presence of leakage. The IP profile shows that the grout curtain proved quite effective within gravels, as there is no continuity between the zones with high chargeability. On the contrary, zones 1, 2 and 3 with low resistivity would correspond to badly grouted areas. These three zones also have higher chargeability due to the presence of clays. Since clays are absent under natural conditions in this specific area, its presence is only explained by an incipient process of internal erosion and deposits.

Hypothetically, the situation could seriously worsen for higher reservoir levels, owing to both the increase in hydraulic gradient and tractive forces in the detected areas, as well as the possible appearance of newly affected areas. Therefore, it is clearly not advisable to raise the reservoir level until remedial measures were carried out.

5.2 Remedial measures for water infiltration

While partially effective in reducing the permeability of the layer of gravels, the execution of the grout curtain (Turkmen, 2003) did not solve the problem of concentrated leakages and stop the incipient process of internal erosion. The repetition of a new grout curtain is ill-advised in light of the presence of multiple paleochannels and the difficulty of grouting them properly. It would therefore be better to build a new concrete cut-off wall –designed by the CHG– taking into account the results offered by the ERT and IP profiles that provide the following important information.

It seem clear that Guadix Formation –impervious clays and conglomerates– does not originate leakages and that the newly designed cut-off wall must be embedded in that geological formation. The designed length of the concrete cut-off wall –856.5 m long– may be excessive.

307 In relation to the area covered by the ERT and IP profiles, between the existing cut-
308 off wall and at 300 m length (Fig. 6) there are no evidences of concentrated leakage.
309 The concrete cut-off wall could therefore be built just between 0 m and 300 m length.
310 However, due to the water could find new paths in the future, the newly designed cut-
311 off wall should be connected with the existing one.

312 According to the obtained results, we propose a new cut-off wall of ~500 m length
313 from the existing one towards the dam. Moreover, the presence of a fault detected must
314 be considered in the new project because it could bring instability or infiltration
315 problems at the future.

316 **6. Conclusions**

317 The mountain ridge close to the left abutment of the Negratín Dam presents leakages
318 that hold a risk of internal erosion. The seepages are caused by the presence of
319 paleochannels embedded in silts that constitute the top of the mountain ridge –from 620
320 m a.s.l. to the surface. Mitigation plans calls for the construction of a concrete cut-off
321 wall crossing this mountain ridge. At this stage, geophysical methods including
322 electrical techniques –ERT and IP– could be applied to evaluate the problem and indeed
323 provided key information about the position of leakages. In addition, these methods
324 helped define limits for the construction of the concrete cut-off wall, which implies
325 lower costs for the problem remediation.

326 Electrical methods, focused on resistivity and induced polarization, were applied
327 along a profile between the water reservoir and the springs with the aim to detect
328 precisely where the infiltrations are taking place. Resistivity methods detected low
329 resistivity areas where infiltration was probable; still, some of these areas entailed
330 further uncertainties about whether the low resistivity in fact corresponded to

infiltration. Induced polarization resolved this issue since the infiltration areas contain clays dragged along by the water-infiltrated thought the paleochannels, detected as zones with high chargeability. Thus, three infiltration areas could be identified at a distance of 90-125-240 m lengths of the electrical profile. Furthermore, the resistivity profile highlights the depth where infiltrations occur, which would be up to 622 m a.s.l.

The information obtained through the electrical profiles made it possible to refine the design of a new concrete cut-off wall in order to mitigate water leakage in the Negratín Dam, with reductions of its dimensions and costs. This research demonstrates that electrical geophysical methods are able to detect water leakage and provide information that helps to improve the design in the construction of mitigation structures preventing internal erosion and future piping phenomena. In addition, this investigation proves the need on geophysical control and monitoring of dam infrastructures for future scientific works for avoiding damage in such structures.

Acknowledgments

The authors wish to thank the *Guadalquivir Hydrographic Confederation* for its collaboration, and to the editor and reviewers for their suggestions that enhanced the quality of the manuscript. This research was funded by project CGL2016-80687-R (AEI/FERDER) of the Spanish Government and by project FCT UID/GEO/50019/2013 – Instituto Dom Luiz. Additional support was given by RNM-148 and RNM-270 research groups of the Junta de Andalucía.

354 **Figure Caption**

355 *Figure 1:* Location of the Negratín Dam. (a) Position of the dam in the Betic Cordillera,
356 S of the Iberian Peninsula, and schematic geological map of the study area.
357 Location of the electrical profile (yellow line) and borehole (red point) are marked
358 inside the study area (red square). (b) Geological cross section on the mountain
359 ridge close to the left abutment in the Negratín Dam. (c) Lithologic column
360 obtained in the drill performed on the study area.

361 *Figure 2:* Paleochannels observed in road slopes at the mountain ridge where the
362 leakages were detected. They have with different sizes: (a) metric scale and (b)
363 decametric scale. Location is marked in Fig. 1.

364 *Figure 3:* Detailed map of the study area. (a) Location of the mountain ridge close to the
365 left abutment in the Negratín Dam. (b) Electrical profile and leaks positions
366 highlighted over orthophoto and topographical contours. The position of the
367 detected springs derived from the leaks on the W side of the mountain ridge are
368 indicated as red stars, and the concrete cut-off wall is marked at the south of the
369 study area.

370 *Figure 4:* Evolution of the storaged water level at the reservoir and its relationship with
371 the leakages flow rate for the period 2009-2017.

372 *Figure 5:* Inversion models of ERT (top) and IP (bottom) profiles with 0.1 DOI index
373 value marked. The electrode spacing is 2.5 m for a 450 m length profile, applying 5
374 times the roll-a-long method. The profile position is indicated in Fig. 2.

375 *Figure 6:* Geological cross section over electrical profiles. The water level where no
376 infiltration occurs and the level at the day of measurements are indicated at 622 and

631 m a.s.l. respectively. The identified water infiltration areas are marked with red dashed ellipses.

REFERENCES

Alfaro, P., Moretti, M. & Soria, J. 1997. Soft-sediment deformation structures induced by earthquakes (seismites) in pliocene lacustrine deposits (Guadix-Baza Basin. Central Betic Cordillera). Eclogae Geologicae Helvetiae, 90, 531-540.

Akande, V.D. 2016. Monitoring of Dam Embankment Using Geoelectrical Techniques at Ojirami Dam, Igarra, Edo State Nigeria. Achievers Journal of Scientific Research, 1, 46-55.

Atallah, N., Shakoor, A. & Watts, C.F. 2015. Investigating the potential and mechanism of soil piping causing water-level drops in Mountain Lake, Giles County, Virginia. Engineering Geology, 195, 282-291, doi: 10.1016/j.enggeo.2015.06.001.

Dahlin, T. & Zhou, B. 2006. Multiple-gradient array measurements for multichannel 2D resistivity imaging. Near Surface Geophysics, 4, 113-123, doi: 10.3997/1873-0604.2005037.

Daily, W., Ramirez, A., Binley, A. & LeBrecque, D. 2004. Electrical resistance tomography. The leading edge, 23, 438-442, doi: 10.1190/1.1729225.

deGroot-Hedlin, C. & Constable, S. 1990. Occam's inversion to generate smooth, two-dimensional models from magnetotelluric data. Geophysics, 55, 1613-1624, doi: 10.1190/1.1442813.

Fell, R., Wan, C.F., Cyganiewicz, J. & Foster, M. 2003. Time for development of internal erosion and piping in embankment dams. Journal of geotechnical and geoenvironmental engineering, 129, 307-314, doi: 10.1061/(ASCE)1090-0241(2003)129:4(307).

Ghobadi, M.H., Khanlari, G.R. & Djalaly, H. 2005. Seepage problems in the right abutment of the Shahid Abbaspour dam, southern Iran. Engineering Geology, 82, 119-126, doi: 10.1016/j.enggeo.2005.09.002.

Gutiérrez, F., Mozafari, M., Carbonel, D., Gómez, R. & Raeisi, E. 2015. Leakage problems in dams built on evaporites. The case of La Loteta Dam (NE Spain), a reservoir in a large karstic depression generated by interstratal salt dissolution. Engineering Geology, 185, 139-154, doi: 10.1016/j.enggeo.2014.12.009.

Jones, J.A.A. & Trudgill, S. 1981. The nature of soil piping: a review of research. Norwich: Geo Books. Vol. 3.

Karaoulis, M., Tsourlos, P., Kim, J.H. & Revil, A. 2014. 4D time-lapse ERT inversion: introducing combined time and space constraints. Near Surface Geophysics, 12, doi: 10.3997/1873-0604.2013004.

LaBrecque, D.J., Ramirez, A.L., Daily, W.D., Binley, A.M. & Schima, S.A. 1996. ERT monitoring of environmental remediation processes. Measurement Science and Technology, 7, 375.

Leroy, P. & Revil, A. 2009. A mechanistic model for the spectral induced polarization of clay materials. Journal of Geophysical Research: Solid Earth, 114, doi: 10.1029/2008JB006114.

Loke, M.H. 2016. Tutorial: 2-D and 3-D Electrical Imaging Surveys. Geotomo Software Company.

Loke, M.H., Acworth, I. & Dahlin, T. 2003. A comparison of smooth and blocky inversion methods in 2D electrical imaging surveys. Exploration Geophysics, 34, 182-187, doi: 10.1071/EG03182.

Loperte, A., Soldovieri, F., Palombo, A., Santini, F. & Lapenna, V. 2016. An integrated geophysical approach for water infiltration detection and characterization at Monte Cotugno rock-fill dam (southern Italy). Engineering Geology, 211, 162-170, doi: 10.1016/j.enggeo.2016.07.005.

Marescot, L., Loke, M.H., Chapellier, D., Delaloye, R., Lambiel, C. & Reynard, E. 2003. Assessing reliability of 2D resistivity imaging in mountain permafrost studies using the depth of investigation index method. Near Surface Geophysics, 1, 57-67, doi: 10.3997/1873-0604.2002007

Marescot, L., Monnet, R. & Chapellier, D. 2008. Resistivity and induced polarization surveys for slope instability studies in the Swiss Alps. Engineering Geology, 98, 18-28, doi: 10.1016/j.enggeo.2008.01.010.

Martínez-Moreno, F.J., Galindo-Zaldívar, J., Pedrera, A., González-Castillo, L., Ruano, P., Calaforra, J.M. & Guirado, E. 2015. Detecting gypsum caves with microgravity and ERT under soil water content variations (Sorbas, SE Spain). Engineering Geology, 193, 38-48, doi: 10.1016/j.enggeo.2015.04.011.

Martínez-Moreno, F.J., Galindo-Zaldívar, J., Pedrera, A., Teixido, T., Ruano, P., Peña, J.A., González-Castillo, L., Ruiz-Constán, A., López-Chicano, M. & Martín-Rosales, W. 2014. Integrated geophysical methods for studying the karst system of Gruta de las Maravillas (Aracena, Southwest Spain). Journal of Applied Geophysics, 107, 149-162, doi: 10.1016/j.jappgeo.2014.05.021.

Martínez-Moreno, F.J., Pedrera, A., Ruano, P., Galindo-Zaldívar, J., Martos-Rosillo, S., González-Castillo, L., Sánchez-Úbeda, J.P. & Marín-Lechado, C. 2013. Combined microgravity, electrical resistivity tomography and induced polarization to detect deeply buried caves: Algaidilla cave (Southern Spain). Engineering Geology, 162, 67-78, doi: 10.1016/j.enggeo.2013.05.008.

Oldenburg, D.W. & Li, Y. 1999. Estimating depth of investigation in dc resistivity and IP surveys. Geophysics, 64, 403-416, doi: 10.1190/1.1444545.

Panthulu, T.V., Krishnaiah, C. & Shirke, J.M. 2001. Detection of seepage paths in earth dams using self-potential and electrical resistivity methods. Engineering Geology, 59, 281-295, doi: 10.1016/S0013-7952(00)00082-X.

Perrone, A., Lapenna, V. & Piscitelli, S. 2014. Electrical resistivity tomography technique for landslide investigation: A review. Earth-Science Reviews, 135, 65-82, doi: 10.1016/j.earscirev.2014.04.002.

Richards, K.S. & Reddy, K.R. 2007. Critical appraisal of piping phenomena in earth dams. Bulletin of Engineering Geology and the Environment, 66, 381-402, doi: 10.1007/s10064-007-0095-0.

Robert, T., Dassargues, A., Brouyère, S., Kaufmann, O., Hallet, V. & Nguyen, F. 2011. Assessing the contribution of electrical resistivity tomography (ERT) and self-potential (SP) methods for a water well drilling program in fractured/karstified limestones. Journal of Applied Geophysics, 75, 42-53, doi: 10.1016/j.jappgeo.2011.06.008.

Sasaki, Y. 1992. Resolution of resistivity tomography inferred from numerical simulation. Geophysical Prospecting, 40, 453-463, doi: 10.1111/j.1365-2478.1992.tb00536.x.

Seed, H.B. & Duncan, J.M. 1987. The failure of Teton dam. Engineering Geology, 24, 173-205, doi: 10.1016/0013-7952(87)90060-3.

Slater, L., Binley, A., Versteeg, R., Cassiani, G., Birken, R. & Sandberg, S. 2002. A 3D ERT study of solute transport in a large experimental tank. Journal of Applied Geophysics, 49, 211-229, doi: 10.1016/S0926-9851(02)00124-6.

Slater, L. & Sandberg, S.W. 2000. Resistivity and induced polarization monitoring of salt transport under natural hydraulic gradients. Geophysics, 65, 408-420, doi: 10.1190/1.1444735.

471 Smalley, I. & Dijkstra, T. 1991. The Teton Dam (Idaho, USA) failure: problems with the use of
472 loess material in earth dam structures. Engineering Geology, 31, 197-203, doi:
473 10.1016/0013-7952(91)90006-7.

474 Soria, J., Fernández, J. & Viseras, C. 1999. Late Miocene stratigraphy and palaeogeographic
475 evolution of the intramontane Guadix Basin (Central Betic Cordillera, Spain): implications
476 for an Atlantic–Mediterranean connection. Palaeogeography, Palaeoclimatology,
477 Palaeoecology, 151, 255-266, doi: 10.1016/S0031-0182(99)00019-X.

478 Suzuki, K., Toda, S., Kusunoki, K., Fujimitsu, Y., Mogi, T. & Jomori, A. 2000. Case studies of
479 electrical and electromagnetic methods applied to mapping active faults beneath the thick
480 quaternary. Engineering Geology, 56, 29-45, doi: 10.1016/S0013-7952(99)00132-5.

481 Turkmen, S. 2003. Treatment of the seepage problems at the Kalecik Dam (Turkey).
482 Engineering Geology, 68, 159-169, doi: 10.1016/S0013-7952(02)00225-9.

483 Unal, B., Eren, M. & Yalcin, M.G. 2007. Investigation of leakage at Ataturk dam and
484 hydroelectric power plant by means of hydrometric measurements. Engineering Geology,
485 93, 45-63, doi: 10.1016/j.enggeo.2007.02.006.

486 Uromeihy, A. & Barzegari, G. 2007. Evaluation and treatment of seepage problems at Chapar-
487 Abad Dam, Iran. Engineering Geology, 91, 219-228, doi: 10.1016/j.enggeo.2007.01.012.

488 Vera, J., Rodriguez-Fernandez, J., Guerra-Merchán, A. & Viseras, C. 1994. La Cuenca de
489 Guadix-Baza. Documents et Travaux de l'IGAL, 14, 1-17.

490 Viseras, C. 1991. Estratigrafía y sedimentología del relleno aluvial de la Cuenca de Guadix
491 (Cordilleras Béticas), Ph.D. Thesis. University of Granada.

492 Wang, Y., Guo, N., Wang, S. & Gu, Y. 2016. Detection of Internal Erosion and Piping in
493 Embankment Dams. International Forum on Energy, Environment and Sustainable
494 Development (IFEESD 2016). pp. 114-122.

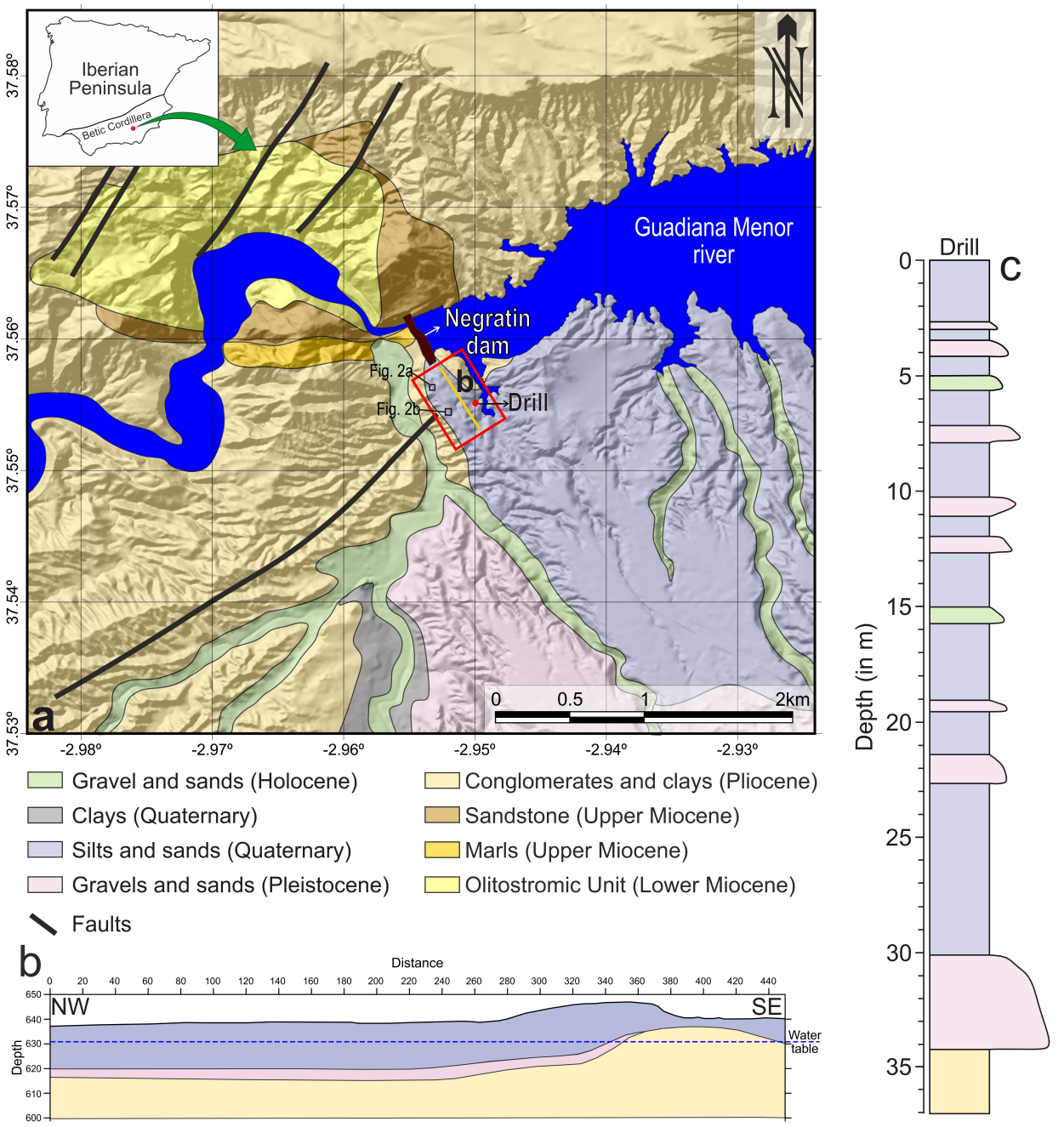
Iberian Peninsula
Betic Cordillera
Guadiana Menor river
Negratin dam
Fig. 2a
Fig. 2b
b
Drill
a
0 0.5 1 2km
37.58°
37.57°
37.56°
37.55°
37.54°
37.53°
-2.98°
-2.97°
-2.96°
-2.95°
-2.94°
-2.93°
Gravel and sands (Holocene)
Clays (Quaternary)
Silts and sands (Quaternary)
Gravels and sands (Pleistocene)
Faults
Conglomerates and clays (Pliocene)
Sandstone (Upper Miocene)
Marls (Upper Miocene)
Olitostromic Unit (Lower Miocene)
b
Distance
NW
SE
Depth
Water table
c
Drill
Depth (in m)

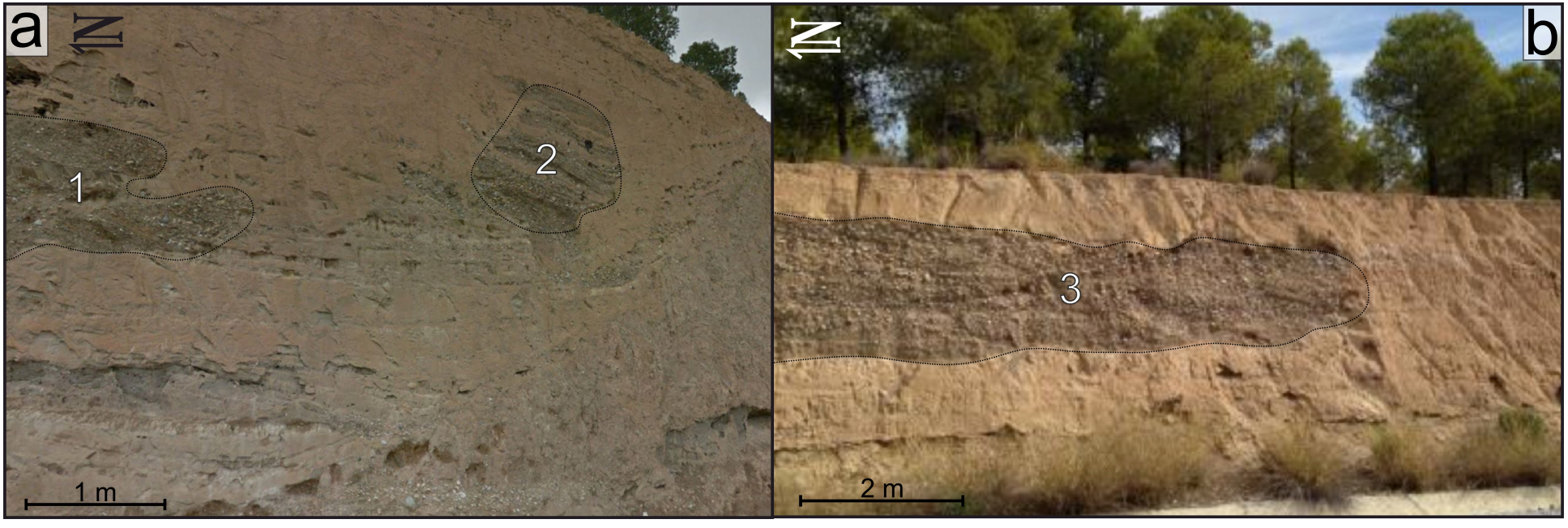
a
N
1
2
1 m
N
b
3
2 m

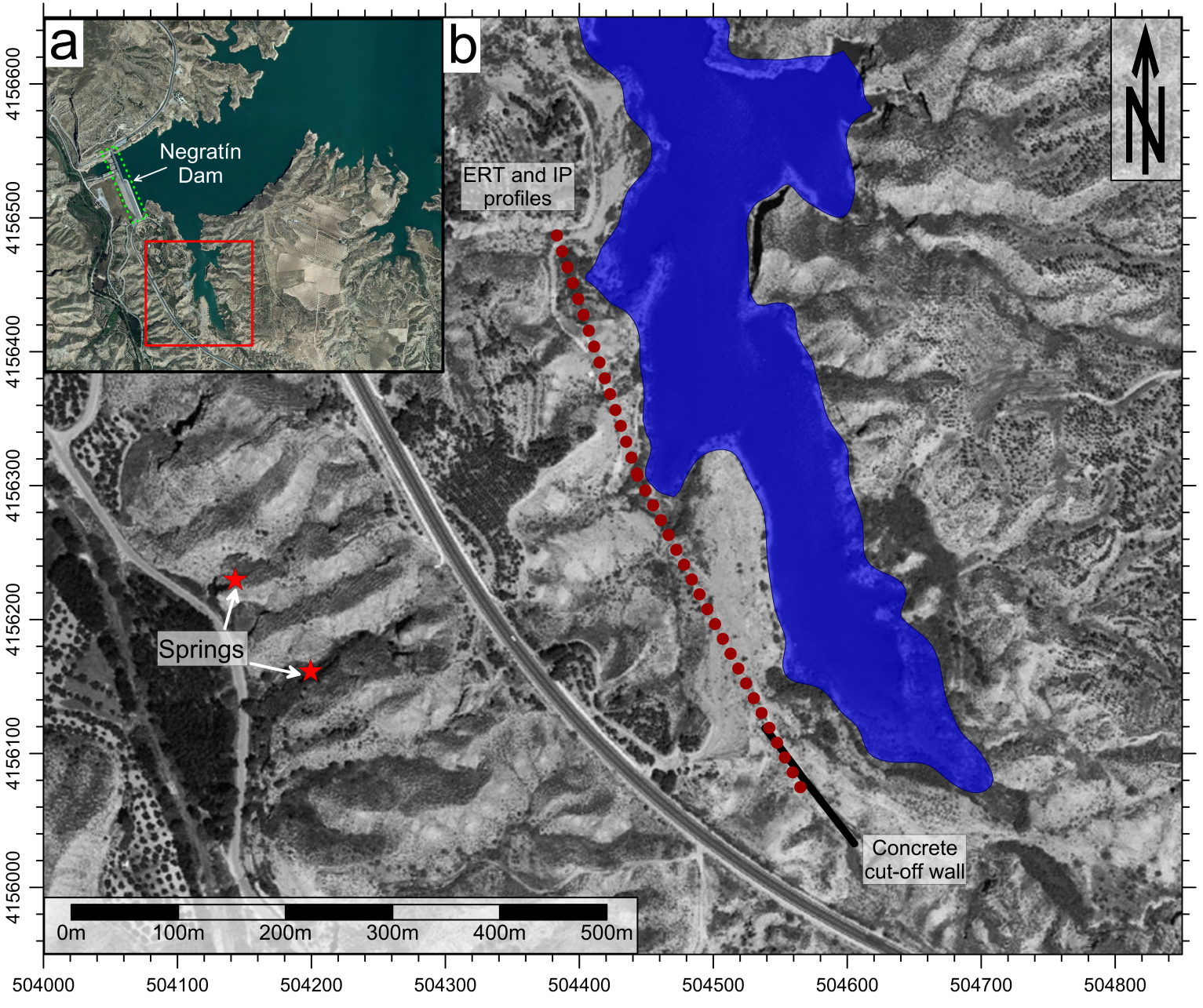
a
Negratín
Dam
b
ERT and IP
profiles
Springs
Concrete
cut-off wall
N
0m
100m
200m
300m
400m
500m
4156600
4156500
4156400
4156300
4156200
4156100
4156000
504000
504100
504200
504300
504400
504500
504600
504700
504800

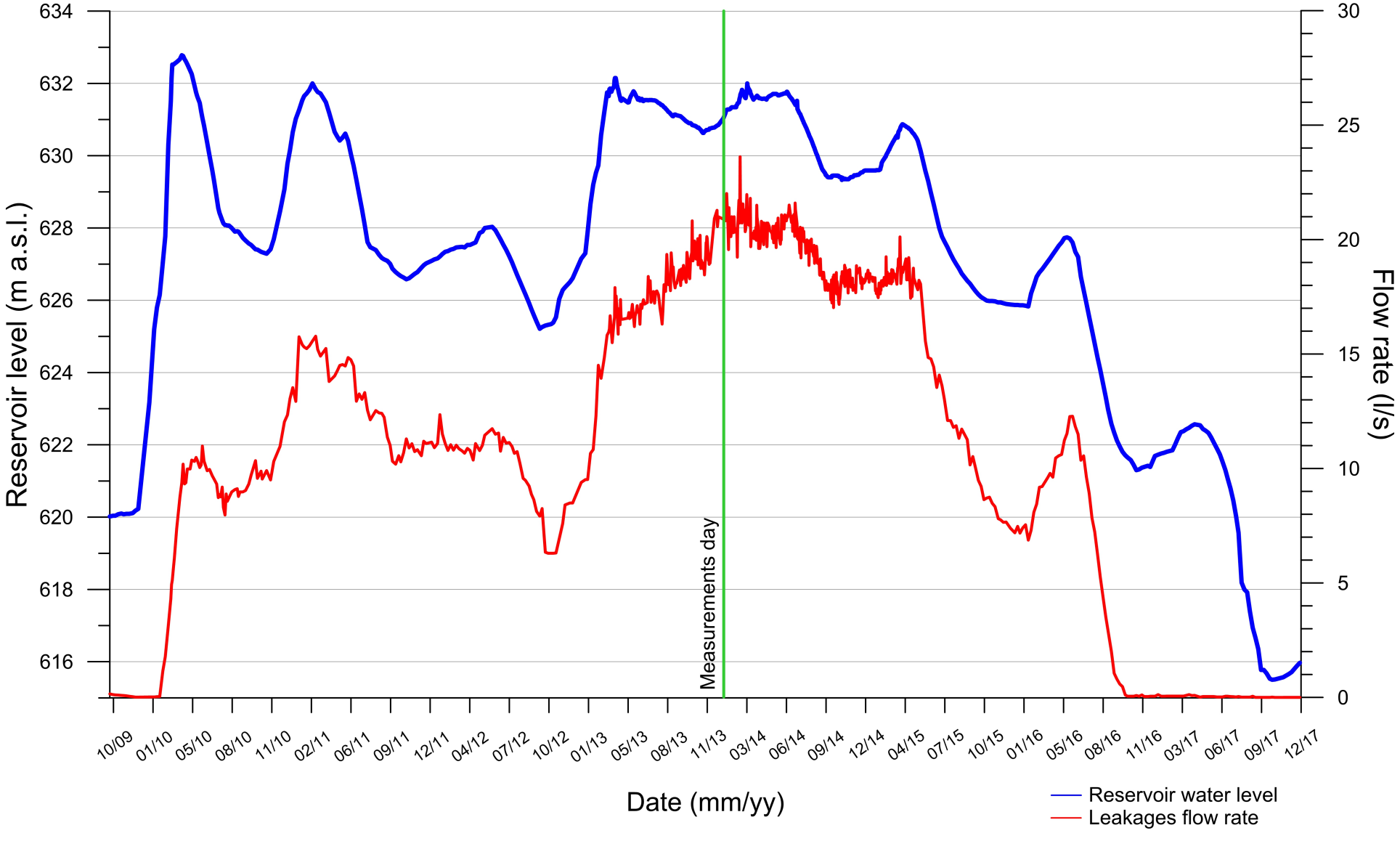
Reservoir level (m a.s.l.)
634
632
630
628
626
624
622
620
618
616
Flow rate (l/s)
30
25
20
15
10
5
0
Measurements day
10/09
01/10
05/10
08/10
11/10
02/11
06/11
09/11
12/11
04/12
07/12
10/12
01/13
05/13
08/13
11/13
03/14
06/14
09/14
12/14
04/15
07/15
10/15
01/16
05/16
08/16
11/16
03/17
06/17
09/17
12/17
Date (mm/yy)
Reservoir water level
Leakages flow rate

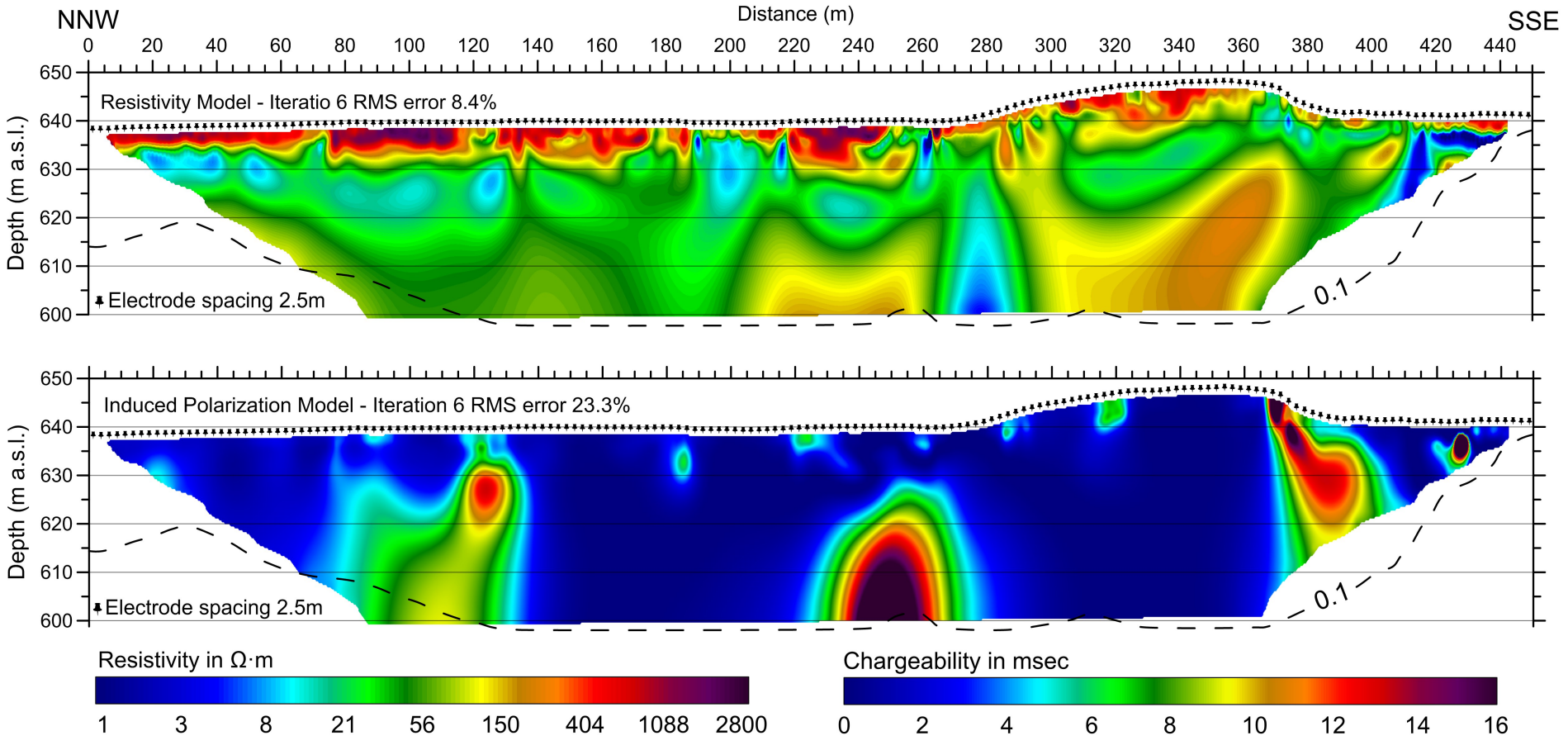
NNW
Distance (m)
SSE
0 20 40 60 80 100 120 140 160 180 200 220 240 260 280 300 320 340 360 380 400 420 440
Depth (m a.s.l.)
650 640 630 620 610 600
Resistivity Model - Iteratio 6 RMS error 8.4%
Electrode spacing 2.5m
0.1
Induced Polarization Model - Iteration 6 RMS error 23.3%
Electrode spacing 2.5m
0.1
Resistivity in Ω·m
1 3 8 21 56 150 404 1088 2800
Chargeability in msec
0 2 4 6 8 10 12 14 16

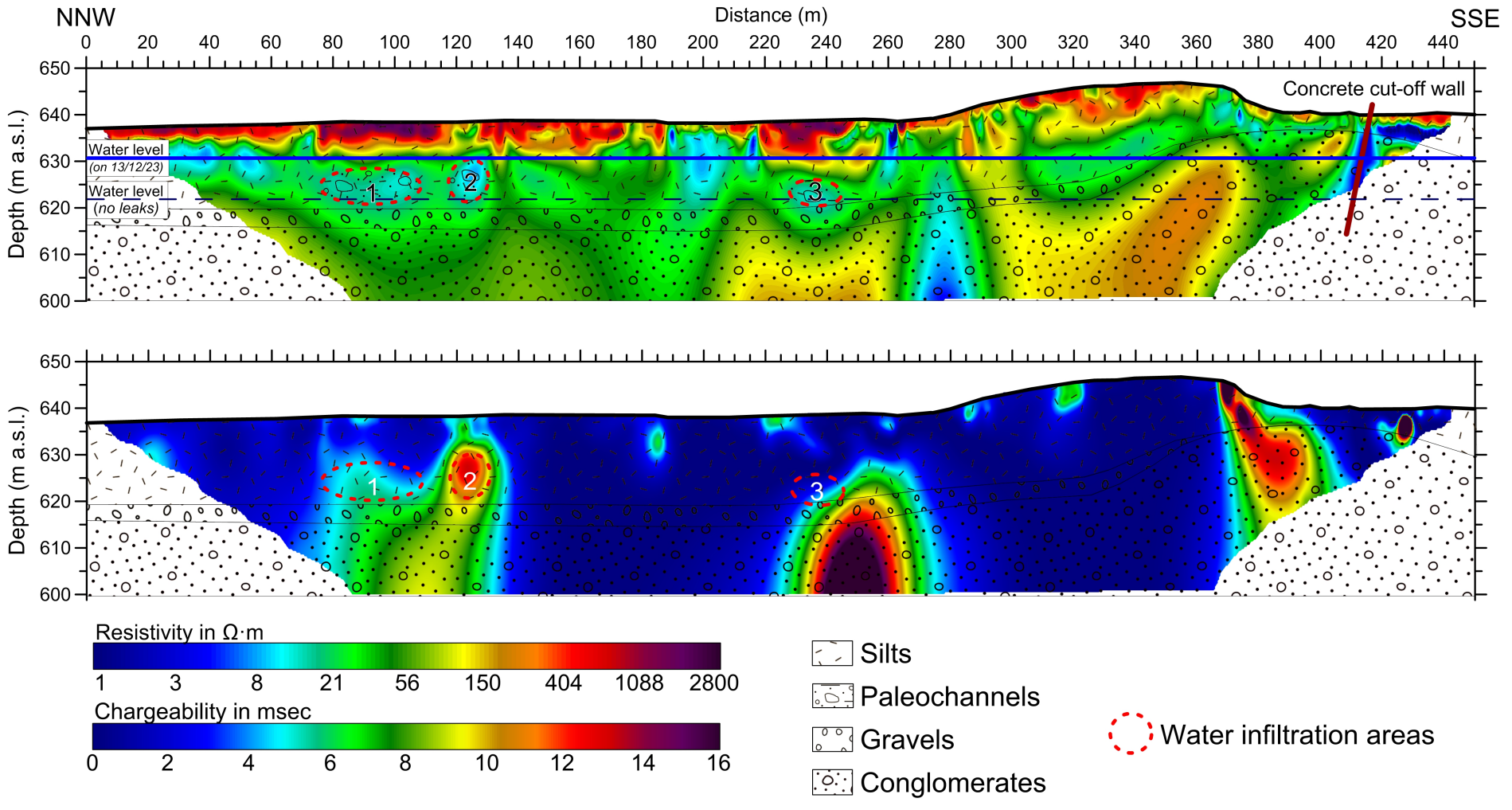
NNW
Distance (m)
SSE
0 20 40 60 80 100 120 140 160 180 200 220 240 260 280 300 320 340 360 380 400 420 440
650 640 630 620 610 600
Depth (m a.s.l.)
Concrete cut-off wall
Water level
(on 13/12/23)
Water level
(no leaks)
1
2
3
Resistivity in Ω·m
1 3 8 21 56 150 404 1088 2800
Chargeability in msec
0 2 4 6 8 10 12 14 16
Silts
Paleochannels
Gravels
Conglomerates
Water infiltration areas